Petrology and U-Th–Pb geochronology of the sapphirine–quartz-bearing metapelites from Rajapalayam, Madurai Block, Southern India: Evidence for polyphase Neoproterozoic high-grade metamorphism

I. Braun, B. Cenki-Tok, Jean-Louis Paquette, M. Tiepolo

Petrology and U–Th–Pb geochronology of the sapphirine–quartz-bearing metapelites from Rajapalayam, Madurai Block, Southern India: Evidence for polyphase Neoproterozoic high-grade metamorphism

I. Braun [a,*], B. Cenki-Tok [b], J.-L. Paquette [c], M. Tiepolo [d]

[a] *Mineralogisch-Petrologisches Institut, Universität Bonn, Poppelsdorfer Schloß, 53115 Bonn, Germany*
[b] *Institut für Geologie, Gruppe Petrologie, Universität Bern, Baltzerstraße 1-3, CH-3012 Bern, Switzerland*
[c] *Département de Géologie, Université Blaise Pascal, 5 rue Kessler, 63038 Clermont-Ferrand, France*
[d] *C.N.R. — Istituto di Geoscienze e Georisorse — Unità di Pavia, Via Ferrata 1, I-27100 Pavia, Italy*

Strongly migmatitic sapphirine-bearing granulites occur as dm- to m-sized enclaves in garnetiferous leucogranites in the southeastern part of the Madurai Block (MB), the largest section of Neoproterozoic crust in the Southern Granulite Terrain of India (SGT). Early mineral assemblages (biotite–sillimanite–quartz, garnet–biotite–quartz) break down via successive dehydration melting reactions to high-T and high-P phase assemblages (e.g. garnet-melt, orthopyroxene–sillimanite-melt, orthopyroxene–cordierite-melt). Melt-consuming reactions along the retrograde path led to partial resorption of garnet to orthopyroxene–sillimanite, orthopyroxene–sapphirine and/or orthopyroxene–cordierite as well as orthopyroxene–sillimanite assemblages to cordierite–biotite–quartz symplectites. The occurrence of UHT metamorphism is indicated by the presence of small inclusions of sapphirine–quartz intergrowths in garnet. This reaction sequence is interpreted in a KFMASH partial petrogenetic grid taking both melt-producing and melt-consuming reactions into account which yields a clockwise heating–cooling–decompression P–T path culminating at 8–11 kbar and 1000–1100 °C.

In-situ U–Th–Pb monazite dating has been performed to more precisely constrain the ages given by chemical electron-microprobe on monazite in various textural positions. Monazite inclusions in garnet often yield a bimodal distribution of early (950–850 Ma) and late Neoproterozoic (600–500 Ma) ages which is in good agreement with the results of U–Pb and EPMA zircon dating in other places of the southeastern Madurai Block. By contrast, monazite inclusions in other mafic minerals (orthopyroxene, cordierite, biotite) or as interstitial phase exclusively yield ages between 550 and 480 Ma. The early Neoproterozoic population is interpreted to reflect the timing of migmatisation and peak UHT metamorphism, whereas the late Neoproterozoic ages are inferred to date cooling and exhumation with granitic magmas to a higher crustal level of the Madurai Block.

Keywords: UHT metamorphism; South India; Sapphirine; Quartz; Monazite; U–Th–Pb geochronology

* Corresponding author.
E-mail addresses: ingo.braun@uni-bonn.de (I. Braun), cenkitok@geo.unibe.ch (B. Cenki-Tok), J.L.Paquette@opgc.univ-bpclermont.fr (J.-L. Paquette), tiepolo@crystal.unipv.it (M. Tiepolo).

1. Introduction

The equilibrium assemblage sapphirine + quartz provides evidence for so-called ultrahigh-temperature (UHT) metamorphism with *P–T* conditions of *ca*. 1000–1100 °C and *ca*. 8–12 kbar. Since their first reports (Dallwitz, 1968; Ellis, 1980) such UHT assemblages in lower crustal rocks have attracted wide interest as their extreme *P–T* conditions indicate unusual geodynamic settings (e.g. Harley, 1998). However, such rocks are often difficult to trace and to identify since the appropriate assemblages usually have been largely replaced by lower-*T* assemblages along the retrograde path and thus may only be preserved as small isolated bodies. Therefore, a major challenge arises when trying to decipher if such retrogressed UHT granulites reflect a single or multiple orogenic cycles. To address such a question requires the combined use of in-situ dating techniques and thermobarometry which allows the *P–T–t* conditions of formation of specific phase assemblages to be constrained.

In this paper, we provide a detailed description of the *P–T* evolution of sapphirine–quartz bearing granulites that have been sampled from a previously undescribed locality in the southeastern part of the Madurai Block, near Rajapalayam in southern India. Tateishi et al. (2004) recently published a first account on the petrology of these rocks and could show that they witnessed UHT conditions. Braun and Appel (2004, 2006) carried out detailed EPMA monazite dating of the granulites and their host rocks. Their results revealed a bimodal distribution of Mid- to early Neoproterozoic and late Neoproterozoic ages in monazite inclusions in the granulite, whereas monazite in the magmatic host rocks exclusively yielded Neoproterozoic values. Based on these reconnaissance studies we present the outcome of U–Pb TIMS and in-situ LA-ICPMS dating of monazite from these rocks in order to constrain the individual ages more precisely and also to check the validity of the early Neoproterozoic values (800–900 Ma) which so far have not been reported from this part of the Madurai Block. Along with this we present new thermobarometric results and petrogenetic grids, which are used to constrain the petrogenesis of the UHT granulites and their role in the Proterozoic tectono-metamorphic evolution of the Madurai Block more comprehensively.

2. Geological setting

The Madurai Block (MB) forms the largest crustal domain in the Proterozoic part of the Southern Granulite

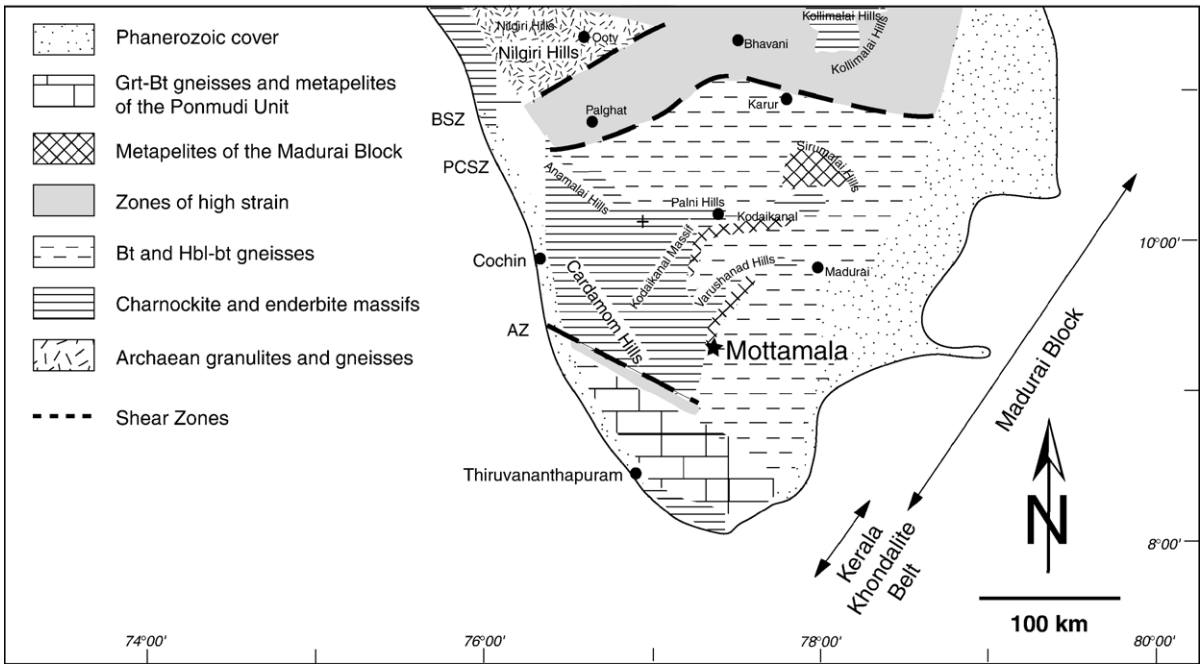

Fig. 1. Simplified geological map of southern India showing the main lithological units and structural elements as well as the position of the sample location (taken from: Braun and Appel (2006). BSZ — Bhavani Shear Zone; PCSZ — Palghat–Cauvery Shear Zone; AZ — Achankovil Zone.

Terrain and is limited to the north by a complex set of tectonic lineaments commonly referred to as the Palghat–Cauvery Shear Zone (PCSZ; Fig. 1).

Details on the crustal architecture and the *P–T–t* evolution of the MB are rare. The Cardamon, Palni and Anamalai Hills (Fig. 1) predominantly consist of massive charnockites and enderbites. Their transition to the gneissic basement in the eastern part of the MB is marked by a steep slope along which numerous metasedimentary complexes occur. These predominantly consist of granulitic metapelites and grt–bt gneisses but also contain lesser quartzites, marbles and calc-silicate rocks.

Isotope and geochronological studies on basement rocks from the MB yield Late Archean to Paleoproterozoic Nd model ages (T_{DM}=*ca*. 2–3 Ga; Harris et al., 1994; Jayananda et al., 1995; Bartlett et al., 1995, 1998; Bhaskar Rao et al., 2003). Pb–Pb zircon evaporation and U–Pb TIMS zircon upper intercept ages between 2 and 2.4 Ga (Jayananda et al., 1995; Bartlett et al., 1995, 1998; Ghosh et al., 2004) are interpreted to reflect a stage of Late Paleoproterozoic magmatism and/or metamorphism. In addition, U–Pb and Pb–Pb zircon ages as well as the results of EPMA dating of monazite from various localities of the MB point to a polyphase Neoproterozoic metamorphic evolution and emphasize the strong imprint of Pan-African high-grade metamorphism (Bartlett et al., 1995; Jayananda et al., 1995; Miller et al., 1997; Bartlett et al., 1998; Santosh et al., 2003; Ghosh et al., 2004).

Tectonically, the Madurai Block is located between two W–E and WNW–ESE late (D3) high strain zones, the Palghat Cauvery Shear Zone (PCSZ) in the north and the Achankovil Zone (AZ) in the south (Cenki and Kriegsman, 2005). The PCSZ is dominated by dextral strike slip deformation (Chetty et al., 2003), whereas the AZ is an inclined zone dominated by intense flattening and pure shear, with a minor reverse component (Cenki and Kriegsman, 2005). The dominant foliation forming event (D1) is synchronous with peak metamorphism. An intermediate deformation phase (D2) is dominated by large scale upright folding of the S1 gneissic layering and affects the regional pattern of the MB. D2 trends are N–S in the western part of the MB (the Kerala highlands), and NE–SW in its north-eastern part (the Tamil Nadu lowlands). These trends are considered to be coeval forming an arc shape pattern (Fig. 1). The studied quarry close to Rajapalayam is located at the hinge of the easternmost inferred arc.

UHT conditions (~1000 °C) at pressures characteristic for the continental lower crust (8–11 kbar) were mainly derived from sapphirine-bearing granulites from the Kodaikanal Massif but occurrences of UHT mineral assemblages are increasingly reported from other places in the MB (Mohan and Windley, 1993; Brown and Raith, 1996; Raith et al., 1997; Sajeev et al., 2004; Tateishi et al., 2004). These estimates of peak metamorphic conditions are slightly higher than those reported for rocks from the Kerala Khondalite Belt (KKB) (Cenki et al., 2002 and references therein) but similar to temperature estimates from marbles further southeast in the MB (Satish-Kumar, 2000). Contrary to this, the vast majority of the gneissic basement in the eastern MB preserves amphibolite-facies assemblages with rare granulite-facies assemblages. It is unclear whether the latter are relics of widespread retrogression

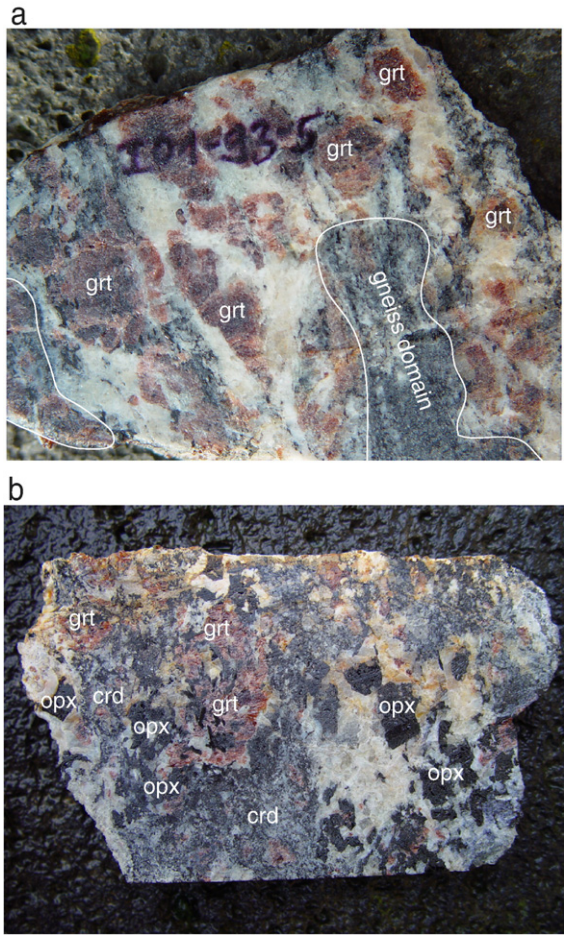

Fig. 2. Hand specimen of migmatitic granulites from the Mottamala quarry. a. Sample (I01-93-5) which has preserved gneissic domains and contains garnet-bearing leucosomes; b. Strongly restitic sample (I02-46-5) with incongruent euhedral orthopyroxene in the leucosome. Large garnet porphyroblast (left) shows partial replacement through coarse-grained cordierite and orthopyroxene. Width of the photographs is 15 cm.

under amphibolite-facies conditions or if granulite-facies conditions were achieved only locally. In addition, the regional significance of UHT assemblages remains ambiguous and it is not known if these reflect the *P–T* evolution of a different crustal fragment which developed independently from the rocks which now seem to host the UHT granulites.

3. Petrography

The sapphirine-bearing granulites presented in this study were found in several active quarries close to the village Mottamala which is situated *ca.* 1 km to the east of Rajapalayam (Fig. 1). They occur as meter-sized enclaves in garnetiferous leucogranites that intruded into granitic (garnet-)biotite gneisses and charnockites. Structures indicate a high degree of migmatisation and melt extraction resulting in strongly restitic and coarse-grained metapelitic granulites (Fig. 2). Folded leucosomes within the enclaves indicate that the metapelites were migmatised prior to leucogranite magma emplacement. This raises the question, whether the migmatisation is related to the generation of the granites or if it represents an earlier and previously unrecognized stage of high-grade metamorphism in this part of the MB.

Hand specimen of the weakly deformed metapelitic granulites display a large textural variability which is controlled by the degree of melt segregation and mineral-melt back reactions (Fig. 2a and b). Those samples that experienced significant melt segregation are dark blueish-black rocks composed of cm-sized cordierite and orthopyroxene crystals with homogeneously distributed sillimanite needles. Samples that still contain remnants of the in-situ melt, host a first generation of large (≤ 1 cm) euhedral orthopyroxene, which most likely formed as an incongruent phase during partial melting. Garnet and biotite are also present in small amounts in most of these samples. Garnet locally forms porphyroblasts but mostly appears as small, relic grains rimmed by retrograde cordierite and, rarely, orthopyroxene. Biotite is present in the mafic domains of all samples and either occurs randomly distributed and fine-grained, or forms medium-grained cluster as breakdown product of cordierite and orthopyroxene.

In thin section, poikiloblastic garnet hosts abundant inclusions of biotite, plagioclase, quartz, opaque and accessory phases. Most spectacular among these inclusion assemblages is the occurrence of tiny (<500 μm) sapphirine–quartz intergrowths (Fig. 3a). Sapphirine is strongly pleochroic, locally optically zoned and contains rare sillimanite inclusions. Locally spinel is associated to sapphirine and quartz without forming intergrowths. Poikilitic cordierite contains inclusions of biotite, sillimanite, garnet, sapphirine and rarely spinel. Large mm-sized orthopyroxene is locally present and contains rare small sillimanite and biotite inclusions. Accessory phases are spinel, zircon, monazite, ilmenite and occasionally rutile. The latter exclusively occurs as inclusion in garnet, whereas the other minerals can be found both as inclusions (predominantly garnet, but also in orthopyroxene, sillimanite and, rarely, quartz and alkali feldspar) and along grain boundaries in the restitic parts and the leucosomes.

The investigated samples display a large variety of reaction textures that are interpreted to reflect the multi-stage consumption of garnet, orthopyroxene–sillimanite and orthopyroxene–cordierite assemblages through repeated interaction with melt and fluid phases. Generally restitic domains have a low amount of quartz whereas retrograde reactions that may have involved a melt phase occur close to leucosome areas. Garnet is commonly strongly embayed and surrounded by symplectites and coronas of variable mineralogy: orthopyroxene and sillimanite (Fig. 3c), orthopyroxene, sillimanite and sapphirine (Fig. 3d), orthopyroxene and sapphirine (Fig. 3e), and orthopyroxene and cordierite (sometimes forming coarse intergrowth mimicking a garnet shape (Fig. 3b), sometimes along cracks in garnet, occasionally with sapphirine inclusions in cordierite; Fig. 3f and g). By contrast, garnet is euhedral at the contact with the leucosome. Quartz is usually found in the leucosome. It forms large anhedral grains and shows undulose extinction. Large orthopyroxene and sillimanite are separated by cordierite (Fig. 3h), cordierite–quartz±sapphirine symplectites, or cordierite–biotite symplectites (Fig. 3i). Locally double coronas (e.g. orthopyroxene–sillimanite symplectites between garnet and cordierite–biotite or orthopyroxene–cordierite symplectites between garnet and biotite) developed with grain-size coarsening from

Fig. 3. Microphotographs (plane polarized light) showing the various reaction textures preserved in the granulites. Scale (lower left corner of each picture) for all photographs is 200 μm. a. Inclusion of a sapphirine–quartz intergrowth in garnet; b. partial replacement of garnet through orthopyroxene + cordierite. The dotted line delineates the shape of the replaced garnet crystal; c. partial replacement of garnet through orthopyroxene + sillimanite; d. strongly embayed garnet relic which is rimmed by symplectitic intergrowths of orthopyroxene, sillimanite and sapphirine; e. symplectitic intergrowth of orthopyroxene and sapphirine replacing garnet; f. symplectitic intergrowth of orthopyroxene and cordierite replacing garnet; g. partial resorption of garnet at the expense of orthopyroxene, cordierite and sapphirine; h. growth of cordierite between orthopyroxene and sillimanite; i. formation of late cordierite and biotite along orthopyroxene–sillimanite grain boundaries and around garnet; j. coronitic growth of cordierite around sapphirine grains in contact with garnet; k. late breakdown of biotite to ilmenite–cordierite intergrowths.

the leucosome towards the garnet. Tiny halos of cordierite between garnet and sapphirine crystals indicate garnet and sapphirine breakdown to cordierite in the presence of melt (Fig. 3j). Orthopyroxene and/or cordierite are separated from the leucosome by irregular biotite aggregates indicating a breakdown of both the first and second generation of orthopyroxene and cordierite into biotite. Additionally, tiny symplectitic intergrowths of ilmenite

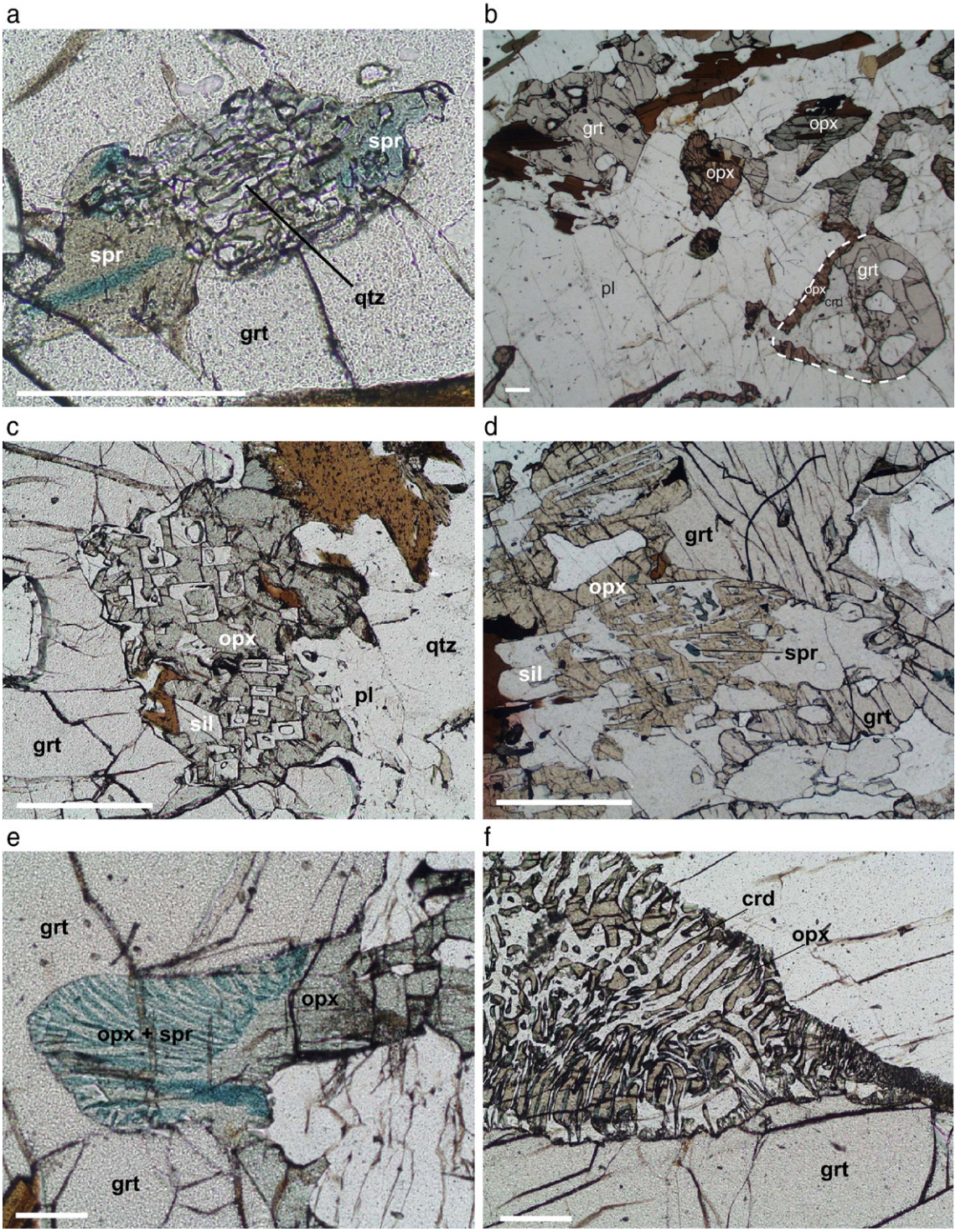

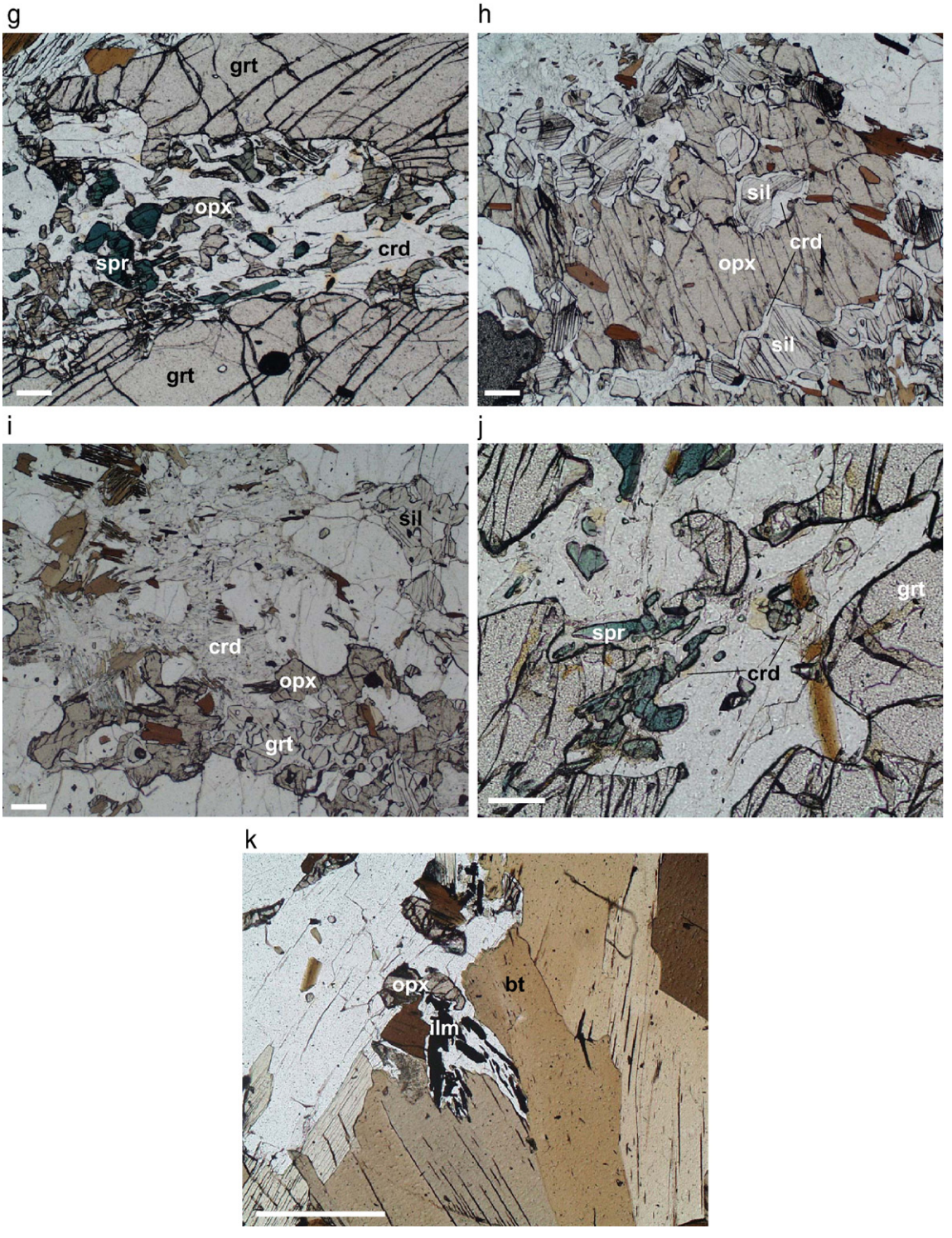

Fig. 3 (*continued*).

and cordierite form at the expense of biotite (Fig. 3k). As the rocks are strongly restitic, leucosomes are rare. In case they occur they are dominated by spindleperthite and quartz. Plagioclase is almost absent and does not play a key role in reaction textures.

4. Mineral chemistry

Mineral compositions have been determined with a Cameca Camebax Microbeam electron probe at the Department of Mineralogy, University of Bonn, operating at 20 kV accelerating voltage and 15 nA beam current. Counting times were 20 s (peak) and 10 s (background). Data processing was performed with the PAP correction procedure (Pouchou and Pichoir, 1984).

Cordierite has a homogeneous magnesium-rich composition (X_{Mg}=0.86–0.87) regardless of its textural position and the reaction through which it was formed. In contrast to this, different *orthopyroxene* generations can be easily distinguished by their chemical composition. Those grains that form subhedral porphyroblasts and symplectites together with sillimanite around garnet yield the highest magnesium abundances (X_{Mg}=0.68–0.73) and Al_2O_3 concentrations (9.22–9.56 wt.-%; Table 1) while intergrowths with cordierite as well as late opx that formed from biotite breakdown have distinctly lower values (X_{Mg}=0.66–0.67; Al_2O_3=7.12–7.25 wt.-%). Chemical zoning has not been observed in any of the different generations.

Garnet is a pyrope–almandine solid solution with both end-members in almost equal amounts (X_{Mg}=0.48–0.51) and very minor contributions from the other constituents. Chemical zoning is very weakly developed and expressed by slightly decreasing X_{Mg} values ($\leq$0.05).

Biotite is TiO_2-rich (5–5.5 wt.-%) and displays significant variations in X_{Mg} values according to its textural position. Biotite in the leucosome, which most likely crystallized from the granitic melt, yields X_{Mg} values of *ca.* 0.69. By contrast, those grains which rimorthopyroxene are significantly more magnesian ($X_{Mg}\sim$0.80).

Sapphirine has a Mg-rich composition in between the 2:2:1 and 7:9:3 end-members and displays strongly varying X_{Mg} (=Mg/(Mg+Fe)) values between 0.76–0.82. These are mainly due to changes in Fe_2O_3 concentrations which are highly variable (3.18–6.80 wt.-%) and negatively correlated with Al_2O_3 and SiO_2. However, there is no observable correlation with its textural context as inclusions in garnet or replacing orthopyroxene–sillimanite intergrowths.

Alkali feldspar has a mesoperthitic composition with high anorthite contents ($\sim$9 mol-%) which points to very high temperatures also during migmatisation.

5. Reaction sequence

The non-equilibrium phase assemblage of the Mottamala rocks comprises garnet (grt), orthopyroxene (opx), cordierite (crd), sapphirine (spr), spinel (spl), biotite (bt), ilmenite (ilm), alkali feldspar (kfs), quartz (qtz) and melt (liq) (mineral abbreviations after Kretz, 1983). Many of these minerals occur in one or more textural contexts and inferred generations. Following the method used to describe the Achankovil cordierite gneisses located further south in the Southern Granulite Terrain (Cenki et al., 2002), all the assemblages can be described in terms of melt-producing and melt-consuming reactions. In the following section, reactions are described in a KFMASH system with K-feldspar in excess (i.e. K-feldspar is not presented and balanced in the reactions).

5.1. Melt-producing reactions

Sapphirine–quartz (Fig. 3a) and sapphirine–spinel–quartz assemblages are only present as inclusions in garnet and therefore do not provide unequivocal textural evidence for the reaction sequence that was responsible for this association. There is evidence that at least some of the garnet was formed quite early at upper amphibolite to granulite-facies conditions during several melt-producing reactions. Small inclusions (10–200 μm) of biotite, quartz, alkali feldspar and fibrolitic sillimanite in garnet porphyroblasts indicate garnet formation through the KFMASH divariant dehydration melting reaction:

$$\mathrm{bt} + \mathrm{sil} + \mathrm{qtz} + \mathrm{kfs} = \mathrm{grt} + \mathrm{liq}. \quad (1)$$

Large (0.2–1 mm) subhedral orthopyroxene crystals containing sillimanite and biotite inclusions may have formed through the multivariate KFMASH melting reaction:

$$\mathrm{bt} + \mathrm{sil}(+\mathrm{qtz} + \mathrm{kfs}) = \mathrm{opx} + \mathrm{liq}. \quad (2)$$

Garnet is broken down at the contact with orthopyroxene and sillimanite crystals but is euhedral at the contact with the leucosome. Large incongruent orthopyroxene and sillimanite aggregates mimicking garnet shapes (Fig. 3c) may have formed via the invariant KFMASH garnet-consuming reaction:

$$\mathrm{grt} + \mathrm{bt}(+\mathrm{qtz} + \mathrm{kfs}) = \mathrm{opx} + \mathrm{sil} + \mathrm{liq}. \quad (3)$$

Large orthopyroxene and cordierite patches containing sillimanite and biotite inclusions (Fig. 3b) could

Table 1
Representative microprobe analyses of mineral phases from the granulite enclaves

Cordierite					
Sample	I02-46-5b				
	11	12	18	21	22
Na_2O	0.01	0.03	0.01	0.04	0.03
MgO	11.92	11.96	11.89	11.68	11.93
Al_2O_3	34.92	34.26	34.83	34.34	34.48
SiO_2	50.54	50.72	49.97	50.60	48.19
FeO	3.09	3.08	3.04	3.25	3.52
Σ	100.62	100.07	99.81	100.12	98.25
Na	0.001	0.005	0.001	0.008	0.006
Mg	1744	1758	1754	1720	1796
Al^{VI}	4040	3984	4062	3999	4105
Si	4961	5004	4945	5000	4868
Fe^{2+}	0.254	0.254	0.252	0.268	0.297
cat.#	11,013	11,008	11,022	11,072	11,084
X_{Mg}	0.87	0.87	0.87	0.87	0.86

Orthopyroxene								
Sample	I02-46-5b						I02-46-5c	
	3	17	19	20	8	13	3	4
	Rim to		Symplectitic intergrowth with					
	grt	grt	crd	bt	sil			
SiO_2	47.92	48.12	48.36	49.00	47.80	47.23	47.76	46.99
TiO_2	0.18	0.16	0.13	0.13	0.22	0.19	0.16	0.17
Al_2O_3	9.22	9.53	7.25	7.12	9.56	9.39	8.71	9.26
Cr_2O_3	0.04	0.02	0.06	0.00	0.03	0.00	0.13	0.11
Fe_2O_3 (c)	3.48	1.23	2.27	1.07	1.68	2.54	4.37	3.78
FeO (c)	15.64	17.51	19.49	19.07	18.08	17.14	15.47	16.60
MnO	0.08	0.02	0.10	0.09	0.11	0.13	0.06	0.04
MgO	23.37	22.51	21.41	22.03	21.88	21.97	23.35	22.19
CaO	0.04	0.01	0.04	0.06	0.04	0.03	0.03	0.03
Σ	99.98	99.12	99.15	98.61	99.43	98.65	100.07	99.21
Si	1749	1772	1805	1827	1763	1755	1746	1740
Ti	0.005	0.004	0.004	0.004	0.006	0.005	0.004	0.005
Al^{IV}	0.251	0.228	0.195	0.173	0.237	0.245	0.254	0.260
Al^{VI}	0.145	0.185	0.124	0.140	0.179	0.166	0.122	0.144
Cr	0.001	0.001	0.002	0.000	0.001	0.000	0.004	0.003
Fe^{3+}	0.096	0.034	0.064	0.030	0.047	0.071	0.120	0.105
Fe^{2+}	0.477	0.539	0.608	0.594	0.558	0.533	0.473	0.514
Mn	0.002	0.001	0.003	0.003	0.003	0.004	0.002	0.001
Mg	1271	1235	1191	1224	1203	1217	1273	1225
Ca	0.001	0.000	0.002	0.002	0.001	0.001	0.001	0.001
cat.#	4000	4000	4000	4000	4000	4000	4000	4000
Wo	0.08	0.02	0.10	0.14	0.08	0.08	0.06	0.06
En	72.64	69.60	66.13	67.22	68.27	69.50	72.87	70.40
Fs	27.28	30.38	33.78	32.64	31.65	30.42	27.08	29.54
X_{Mg}	0.73	0.70	0.66	0.67	0.68	0.70	0.73	0.70

Table 1 (*continued*)

Garnet

Sample	I02-46-5b	I02-46-5c	I02-46-5b		I02-46-5c
	7	1	2	14	2
	Core		Rim to		
			opx	opx	opx
SiO_2	39.69	39.90	39.37	38.97	39.16
TiO_2	0.02	0.01	0.04	0.00	0.02
Al_2O_3	22.79	22.71	23.02	22.72	22.96
Cr_2O_3	0.02	0.04	0.00	0.03	0.03
Fe_2O_3 (c)	0.00	0.58	0.90	0.57	1.85
FeO (c)	23.62	22.94	22.76	23.52	22.77
MnO	0.26	0.21	0.30	0.23	0.26
MgO	12.69	13.40	13.10	12.38	13.02
CaO	0.56	0.53	0.55	0.60	0.43
Σ	99.65	100.32	100.04	99.04	100.52
Si	2992	2982	2955	2964	2933
Ti	0.001	0.001	0.002	0.000	0.001
Al^{IV}	0.008	0.018	0.045	0.036	0.067
Al^{VI}	2016	1982	1990	2001	1960
Cr	0.001	0.002	0.000	0.002	0.002
Fe^{3+}	0.000	0.032	0.051	0.033	0.104
Fe^{2+}	1489	1434	1428	1496	1427
Mn	0.017	0.013	0.019	0.015	0.016
Mg	1425	1493	1465	1404	1454
Ca	0.045	0.042	0.044	0.049	0.035
cat.#	7995	8000	8000	8000	8000
Pyrope	47.89	50.06	49.55	47.36	49.60
Almandin	50.02	48.08	48.32	50.48	48.67
Spessartine	0.56	0.45	0.65	0.51	0.56
Andradite	0.00	1.61	2.49	1.61	5.05
Uvarovite	0.06	0.12	0.01	0.09	0.09
Grossulaire	1.47	−0.30	−1.01	−0.05	−3.96
X_{Mg}	0.49	0.51	0.51	0.48	0.50

Alkalifeldspar

Sample	I02-46-5b	I02-46-5c
	1	7
		Rim to
	Leucosome	opx–sil
SiO_2	65.37	64.60
Al_2O_3	20.86	20.20
CaO	1.97	1.12
Na_2O	6.51	6.11
K_2O	6.23	8.87
Σ	101.11	101.03
Si	2902	2906
Al	1091	1071
Ca	0.094	0.054
Na	0.560	0.533
K	0.353	0.509
cat.#	5006	5078
Ab	55.65	48.63
An	9.30	4.93
Or	35.06	46.45

(continued on next page)

Table 1 (*continued*)

Sample	I02-46-5c	
	5	6
SiO_2	36.19	37.27
TiO_2	5.38	5.01
Al_2O_3	15.46	15.99
Cr_2O_3	0.06	0.08
Fe_2O_3 (c)	0.00	0.00
FeO (c)	12.19	8.11
MnO	0.00	0.07
MgO	15.68	18.79
CaO	0.01	0.00
Na_2O	0.18	0.19
K_2O	10.04	10.46
H_2O	4.44	4.56
Σ	99.66	100.56
Si	2444	2449
Ti	0.273	0.248
Al^{IV}	0.675	0.688
Al^{VI}	0.556	0.551
Cr	0.003	0.004
Fe^{3+}	0.000	0.000
Fe^{2+}	0.689	0.446
Mn	0.000	0.004
Mg	1579	1841
Ca	0.001	0.000
Na	0.024	0.024
K	0.865	0.877
OH	2000	2000
cat.#	9110	9132
X_{Mg}	0.30	0.19

Sapphirine

Sample	I02-46-5b				
	4	5	9	15	16
	Inclusion in				
	grt	sil	sil	grt	grt
SiO_2	12.56	12.08	13.17	13.26	13.05
TiO_2	0.06	0.05	0.07	0.07	0.13
Al_2O_3	58.00	57.75	59.24	59.74	59.88
Cr_2O_3	0.13	0.14	0.12	0.10	0.07
Fe_2O_3 (c)	5.69	6.80	3.71	3.18	3.88
FeO (c)	6.53	6.75	8.56	8.28	7.49
MnO	0.05	0.01	0.00	0.00	0.00
MgO	15.69	15.21	15.15	15.39	15.69
Σ	98.73	98.80	100.02	100.03	100.24
Si	1536	1487	1594	1599	1569
Ti	0.006	0.005	0.006	0.006	0.012
Al	8375	8376	8450	8492	8487
Cr	0.013	0.014	0.011	0.010	0.007
Fe^{3+}	0.525	0.630	0.338	0.288	0.351
Fe^{2+}	0.669	0.695	0.867	0.835	0.753
Mn	0.005	0.001	0.000	0.000	0.000
Mg	2866	2791	2733	2767	2813
cat.#	14,000	14,000	14,000	14,000	14,000
X_{Mg}	0.81	0.80	0.76	0.77	0.79

have formed via a multivariant KFMASH reaction related to the univariant KFMASH reaction:

$$bt + sil(+qtz) = opx + crd + liq. \quad (4)$$

The occurrence of sapphirine–quartz inclusions in garnet (Fig. 3a) may be explained in three different ways. If garnet exclusively formed through reaction (1) it may be assumed that spr–qtz formed previously during a stage of UHT metamorphism and then became enclosed in garnet. We consider this hypothesis as unlikely since it would require that the symplectitic intergrowths of sapphirine and quartz did not recrystallize during cooling from UHT conditions and the subsequent garnet-forming reactions.

Alternatively, sapphirine–quartz intergrowths could have formed after the growth of garnet at UHT conditions and a possible mechanism to explain this would be the reaction between the host garnet and sillimanite inclusions following the multivariate KFMASH reaction:

$$grt(+sil) = spr + qtz. \quad (5a)$$

Finally, sapphirine–quartz intergrowths and host garnets could both have formed at UHT conditions and with increasing temperature in domains with high bulk Al/Si ratios. First, intergrowths were formed through the univariant KFMASH reaction

$$opx + crd + sil = spr + qtz + liq. \quad (5b)$$

At even higher temperatures garnet (over)growth on them could have taken place in such domains according to the multivariate KFMASH reaction

$$opx + sil + qtz = grt. \quad (5c)$$

5.2. Melt-consuming reactions

The large garnet grains always display strongly embayed grain boundaries and are rimmed by coronas of various breakdown assemblages. Among these, the most common are coarse-grained and occasionally euhedral orthopyroxene–sillimanite intergrowths (Fig. 3c and d) which formed according to the KFMASH divariant reaction

$$grt + liq(+spr) = opx + sil \quad (6)$$

which is located at slightly higher pressure than the univariant reaction opx+sil+kfs=grt+spr+qtz+liq. In

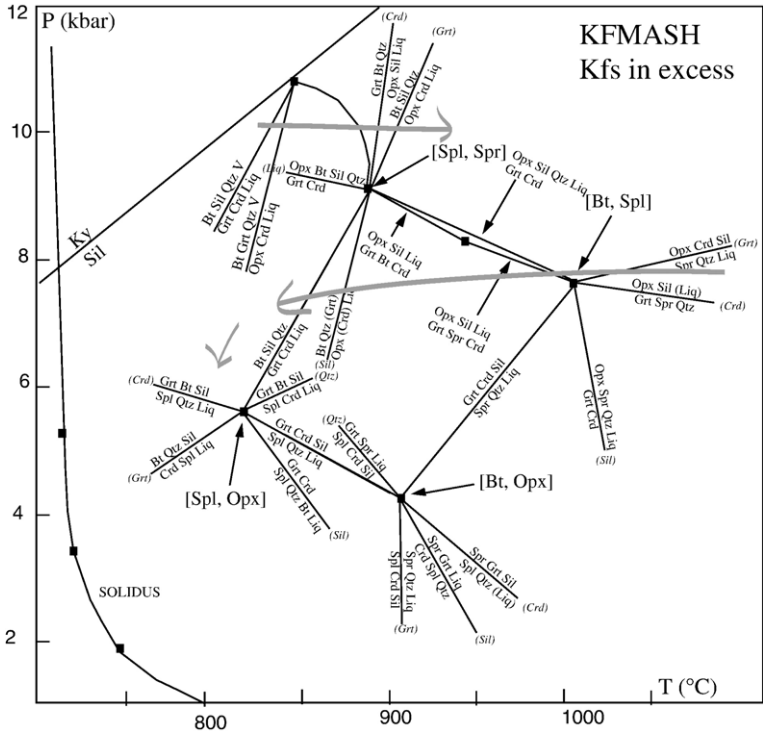

Fig. 4. Partial petrogenetic grid locating in P–T space the qualitative pseudosection presented in Fig. 5. The arrows indicate the inferred P–T path (see text for explanations). Abbreviations after Kretz (1983).

addition to this, garnet replacement has also led to the development of coarse to fine-grained symplectitic orthopyroxene–sapphirine (Fig. 3e) and orthopyroxene–cordierite-(sapphirine) assemblages (Fig. 3d, f, g). Appropriate multivariate KFMASH reactions are

$$\mathrm{grt} + \mathrm{liq} = \mathrm{opx} + \mathrm{spr} \quad (7a)$$

and

$$\mathrm{grt} + \mathrm{liq} = \mathrm{opx} + \mathrm{crd}(+\mathrm{spr}) \quad (7b)$$

which are located on the lower pressure side of the orthopyroxene–sillimanite stability joint.

Locally, tiny halos of cordierite between sapphirine and garnet crystals (Fig. 3j) close to the quartzofeldspathic matrix indicate a multivariate reaction closely related to the KFMASH divariant reaction:

$$\mathrm{grt} + \mathrm{spr} + \mathrm{liq} = \mathrm{crd} + \mathrm{qtz}. \quad (7c)$$

Breakdown of the various orthopyroxene–sillimanite-bearing assemblages leads to the growth of cordierite as well as several symplectitic intergrowths involving cordierite and other phases through a variety of di- or trivariant melt-mineral KFMASH back reactions (Fig. 3h and i) located above the orthopyroxene–sillimanite joint:

$$\mathrm{opx} + \mathrm{sil} + \mathrm{liq} = \mathrm{crd} \quad (8a)$$

$$\mathrm{opx} + \mathrm{sil} + \mathrm{liq} = \mathrm{crd} + \mathrm{bt}(+\mathrm{qtz}) \quad (8b)$$

$$\mathrm{opx} + \mathrm{sil} + \mathrm{liq} = \mathrm{crd} + \mathrm{qtz}. \quad (8c)$$

Late biotite forms from the breakdown of orthopyroxene and cordierite in the presence of melt according to the high variance reactions

$$\mathrm{opx} + \mathrm{liq} = \mathrm{bt} \quad (9a)$$

and

$$\mathrm{crd} + \mathrm{liq} = \mathrm{bt} \quad (9b)$$

which are related to the KFMASH univariant dehydration melting reaction bt+qtz+grt+kfs=opx+crd+liq located under the [spinel, sapphirine] KFMASH invariant point. However, locally, the reverse of Eq. (9a) is also observed and expressed by tiny orthopyroxene rims around biotite which indicates a reaction

$$\mathrm{bt} + \mathrm{liq} = \mathrm{opx} + \mathrm{liq}. \quad (9c)$$

Finally, tiny symplectitic intergrowths of ilmenite and cordierite formed at the expense of biotite (Fig. 3k).

6. *P–T* data and petrogenetic grids

6.1. Construction of the petrogenetic grids

In addition to the melt phase that is present under ultra high temperature conditions, eight major phases are recognized: garnet, orthopyroxene, cordierite, sapphirine, spinel, biotite, k-feldspar and quartz. At least 6 major components are necessary to describe the system: K_2O–FeO–MgO–Al_2O_3–SiO_2–H_2O (KFMASH). The choice of phases and chemical system is described in detail in Cenki et al. (2002).

The petrogenetic grids are presented in Figs. 4 and 5. The *P–T* location of KFMASH invariant points [spinel, sapphirine], [biotite, spinel] is constrained by stability calculations (Spear et al., 1999; Kelsey et al., 2004) and experimental results (Carrington and Harley, 1995). Most of the corresponding univariant lines are taken from experimental and topological data (McDade and Harley, 2001). The KFMASH univariant reactions bt+sil+qtz=grt+crd+liq and bt+qtz+grt=opx+crd+liq have the same *P–T* location as in Cenki et al. (2002). The remaining univariant lines and the divariant bundles around each of these critical univariant lines have been balanced with matrix analysis in the KFMASH system (using the following X_{Mg}: garnet — 0.5, cordierite — 0.85, orthopyroxene — 0.7, sapphirine — 0.77) and built according to the geometrical rules of Schreinemaker analysis (Zen, 1966). The reaction sequence is well described around the [biotite, spinel] and [spinel, sapphirine] KFMASH invariant points. Due to the way the grid has been built, the reactions cordierite-absent ((crd)) and liquid-absent ((liq)) usually appear degenerate but in reality the divariant reactions (crd) and (liq) would involve a slight proportion of melt or cordierite, respectively. In addition, k-feldspar singularities are not treated in detail and k-feldspar is therefore considered in excess in the petrogenetic grids.

The location of the solidus, the kyanite–sillimanite boundary and the three related reactions involving a vapor phase (*V*) as reactant are taken from Kelsey et al. (2004).

6.2. Description of the P–T path and thermobarometry

Based on the calculated KFMASH grids, the interpretation of the mineral assemblages and reaction textures yields a clockwise *P–T* path, segmented in three parts: heating, cooling, decompression (Figs. 4 and 5).

During prograde heating, melt-producing reactions ((1)–(4) and (5b)) produce one or more incongruent phases (garnet, cordierite, orthopyroxene, sillimanite)

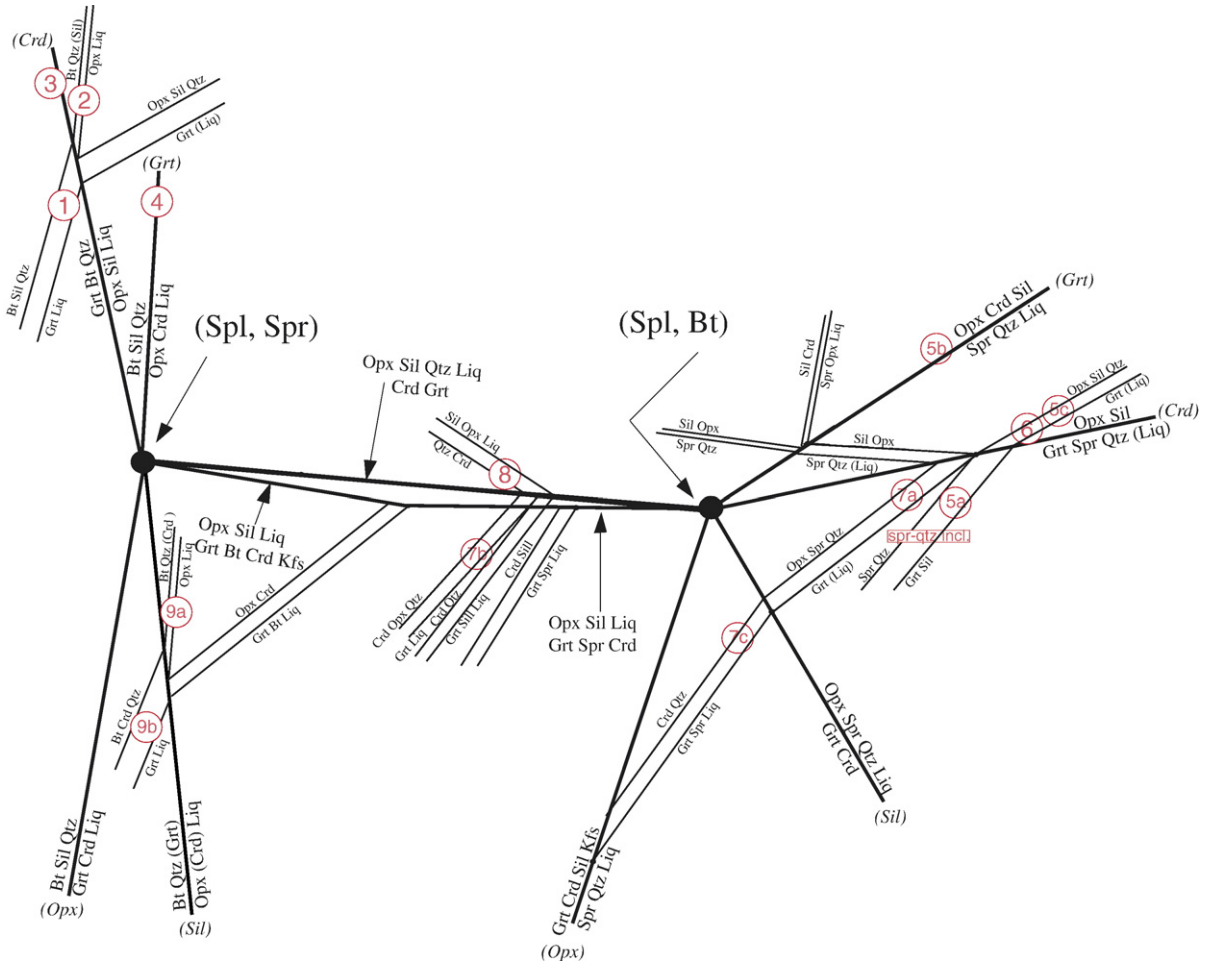

Fig. 5. Qualitative partial pseudosection in a PT space (P vertical axis, T horizontal axis) presenting the reactions observed in the sapphirine–quartz rocks from Mottamala. Invariant KFMASH points (points) and univariant KFMASH lines (thick lines) are taken from the literature (Carrington and Harley, 1995; McDade and Harley, 2001; Cenki et al., 2002; Kelsey et al., 2004). Divariant KFMASH fields (thin lines) built with Schreinemakers geometrical rules (Zen, 1966). Kfs is in excess. See text for further explanations.

along with melt above the [spl, spr] invariant point (i.e. within the stability field of orthopyroxene and sillimanite >8.8 kbar) and below the kyanite–sillimanite joint (Fig. 5). The early assemblage sapphirine–quartz formed at much higher *T* (in the biotite-out field) either from destabilization of sillimanite inclusions in garnet or the breakdown of orthopyroxene–sillimanite–cordierite assemblages.

The retrograde path (Fig. 5) is marked by a series of melt-consuming reactions indicating cooling related to the breakdown of garnet (reactions (6)–(7c)) or orthopyroxene–sillimanite assemblages (reactions (8a)–(8c)). These trends are located around the [spinel, biotite] invariant point and on both sides of the orthopyroxene–sillimanite joint. Reactions (6)–(7c) consume little melt as the crd- and liq-absent reactions are almost degenerate. The shallow slope of this cooling path is further constrained by the absence of sapphirine–quartz retrograde assemblages and spinel in coronas or symplectites. The path has to be isobaric above the [spl, opx] and [bt, opx] invariant points and below the [spinel, sapphirine] and [spinel, biotite] invariant points (Fig. 4) until decompression takes place (i.e. below 6 kbar; 850 °C; Raith et al., 1997). This last stage is not visible in spinel-free assemblages but may be recorded in rocks that have a higher alumina content.

Breakdown of orthopyroxene and cordierite in the presence of melt (reactions (9a) and (9b)) occurs at the end of this cooling path and indicates the onset of decompression. Evidences for the shape of the decompression path are rare. It may follow an isothermal

Table 2
Results of Al-in-orthopyroxene coexisting with garnet thermobarometry (Harley and Green, 1982)

	Garnet analyses		
	2	7	14
X_{Ca}	0.01	0.02	0.02
X_{Fe}	0.49	0.50	0.51
X_{Mg}	0.49	0.48	0.47
Fe/Mg	0.99	1.04	1.08
	Orthopyroxene analyses		
	3	8	13
$X_{Al,M1}$	0.20	0.21	0.21
X_{Fe}	0.29	0.32	0.32
X_{Mg}	0.71	0.68	0.68
Fe/Mg	0.41	0.46	0.47
K	0.17	0.17	0.17
ΔVr	−212.10	−213.03	−212.80
T (°C)	1075	1075	1075
T (K)	1348	1348	1348
P (kbar)	11.32	10.74	10.77

decompression arrow parallel to the univariant reaction bt+sil+qtz=grt+crd+kfs+liq on its low temperature side.

Semi-quantitative estimations (Fig. 4) yield a heating–cooling P–T path culminating at 8–11 kbar and 1000–1100 °C. Thermobarometric calculations using aluminium in orthopyroxene coexisting with garnet (Harley and Green, 1982) gave estimations for the peak of metamorphism at ~11 kbar at 1075 °C (Table 2).

7. Geochronology

Electron-microprobe (EPMA) dating of monazite was carried out on the thin sections which were prepared for drilling of single monazite grains. The main purpose of this step was to identify grains that host a pre-Pan-African (>600 Ma) age population, which then could be chosen for more precise U–Pb TIMS dating. We therefore concentrated on samples which previously have been investigated carefully by EPMA dating (Braun and Appel, 2006). The results of these investigations confirmed the earlier studies and show that the host granite of the enclaves (sample I02-8-5a) exclusively contains monazite with Neoproterozoic ages (470–570 Ma). By contrast, monazites in the two granulite samples (I01-93-5, I02-46-5) display a large range of late to early Neoproterozoic ages (Braun unpubl. data; Braun and Appel, 2006).

According to this, U–Pb ID-TIMS (method after Paquette and Pin, 2001, all the errors quoted at the 2σ level) dating of separated monazite grains from the granite sample I02-8-5a gave four individual but concordant Neoproterozoic III to Cambrian ages between 551±1 and 493±1 Ma (Fig. 6, Table 3). They are in perfect agreement with similar concordant U–Pb ID-TIMS ages (551±1–481±5 Ma) from micro-drilled monazite inclusions (method described in Paquette et al., 2004) in orthopyroxene and quartz from the spr–qtz-bearing granulite sample I02-46-5 (Fig. 6). A monazite inclusion in garnet (Fig. 7a) was analysed in the granulite sample I01-93-5 for U–Th–Pb geochronology with laser ablation (LA)-ICPMS. The instrument couples a 193 nm ArF excimer laser (type GeoLas102-MicroLas) with a sector filed ICPMS (type Element I from ThermoFinnigan). The analytical method is basically that developed for zircon by Tiepolo (2003) and later modified for monazite by Paquette and Tiepolo (in press). Five spot analyses using a spot size of 5 μm, 12 J cm^{-2} of energy density and 3 Hz of repetition rate of the laser were carried out on the monazite crystal. Time resolved signals were carefully inspected to evaluate the presence of common Pb, inclusions or perturbations related to fractures. Data reduction was carried out with the Glitter software (van Achterbergh et al., 2001) and all analytical errors were fully propagated. Each analysis is thus retained accurate within the quoted errors (Table 4). The 5 analyses give consistent Th–Pb and U–Pb ages. The mean $^{208}Pb/^{232}Th$ age is 501±12 Ma (2σ, MSWD=0.98), the mean $^{206}Pb/^{238}U$ age is 497±10 Ma (2σ, MSWD=1.5) and the three concordant U–Pb ages (Fig. 7b, Table 4) yield a mean concordia age of 497±12 Ma (2σ, MSWD=9.2). In contrast to this, U–Pb ID-TIMS dating of a micro-drilled

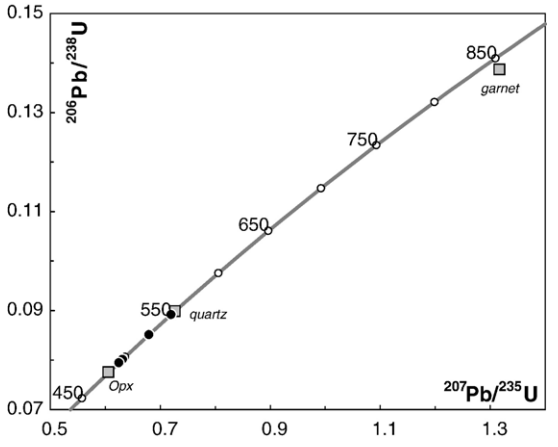

Fig. 6. Concordia diagram showing the results of U–Pb monazite dating. Black dots represent monazite grains from the granite (sample I02-8-5a) that hosts the metapelitic enclaves, squares are monazite inclusions in minerals from the enclave (sample I02-46-5).

Table 3
Results of U–Pb TIMS dating of monazite grains from the granite host (mnz 1–4) and the granulite (mnz 5–7)

No.	Wt.	U	Pb rad	^{206}Pb	^{208}Pb	^{206}Pb	^{207}Pb	^{207}Pb	^{206}Pb	^{207}Pb	^{207}Pb	Correlation
	(μg)	(ppm)	(ppm)	^{204}Pb	^{206}Pb	^{238}Pb	^{235}Pb	^{206}Pb	^{238}Pb	^{235}Pb	^{206}Pb	Coefficient
						Atomic ratios			Apparent ages (Ma)			
mnz1 I02-8-5a	13	1064	1338	5382	15.898	0.08515 (0.16%)	0.6796 (0.27%)	0.05789 (0.20%)	527	527	526	0.66
mnz2 I02-8-5a	20	3365	1021	24833	3.8653	0.08919 (0.14%)	0.7199 (0.15%)	0.05855 (0.05%)	551	551	550	0.95
mnz3 I02-8-5a	10	576	622	534	13.912	0.08015 (0.21%)	0.6315 (0.37%)	0.05714 (0.30%)	497	497	497	0.60
mnz4 I02-8-5a	11	701	506	3537	9.3633	0.07948 (0.17%)	0.6246 (0.28%)	0.05700 (0.22%)	493	493	492	0.64
mnz5 I02-46-5 opx	1	757	1625	819	30.202	0.07756 (1.06%)	0.6055 (1.97%)	0.05662 (1.59%)	482	481	477	0.59
mnz6 I02-46-5 qtz	1	1960	1035	4565	5.6915	0.08987 (0.15%)	0.7266 (0.23%)	0.05864 (0.17%)	555	555	554	0.68
mnz7 I01-93-5 grt	5	3486	1699	21,291	2.9842	0.1387 (0.15%)	1.3168 (0.15%)	0.06884 (0.04%)	837	853	894	0.96

Monazite grains were not mechanically abraded. The isotopic ratios are corrected for mass discrimination (0.1±0.015% per amu for Pb and U), isotopic tracer contribution and analytical blanks: 5.5±3.5 pg for Pb and less than 1 pg for U. Initial common Pb is determined for each fraction in using the Stacey and Kramers (1975) two-step model.

monazite inclusion in garnet from this sample gave a slightly discordant early Neoproterozoic age, the corresponding $^{207}Pb/^{206}Pb$ minimum age of which is 894±1 Ma (Fig. 6, Table 3).

8. Discussion

Since its first description in southern India by Grew (1982) sapphirine has been reported from an increasing number of rock types and occurrences in the eastern part of the Madurai Block (Santosh et al., 2004; Tateishi et al., 2004 and references therein). In particular, the recognition of sapphirine–spinel and sapphirine–quartz provided evidence for a stage of high- to ultra-high-temperature metamorphism in southern India. However, it is still unclear whether the reaction textures and phase assemblages observed in these rocks reflect a single stage metamorphic evolution or belong to independent orogenic events.

Tateishi et al. (2004) first presented sapphirine–quartz assemblages in rocks from the Mottamala quarry, which are reported here. From phase petrology and thermobarometric calculations they inferred minimum *P–T* conditions of 8 kbar and 1050 °C followed by an initial stage of isobaric cooling and the onset of decompression at temperatures exceeding 900 °C. The results presented in this study do not entirely support this view. Whereas the *P–T* conditions for the peak of metamorphism in our study are fairly similar to those of Tateishi et al. (2004), our results indicate protracted near-isobaric cooling before decompression starts at temperatures of *ca*. 800 °C. The main reasons for this discrepancy are (i) the widespread occurrence of orthopyroxene–sillimanite assemblages in our samples which requires a cooling path well above the [spinel, biotite] invariant point, (ii) the occurrence of back reactions of garnet and orthopyroxene with melt-producing biotite, cordierite and quartz symplectites that marks the end of the cooling path at *ca*. 850 °C and 8 kbar and (iii) the fact that we take a melt phase (e.g. quartz component of the melt) instead of a solid phase (e.g. quartz) into account for most of the retrograde reactions. Kriegsman and Hensen (1998) demonstrated that this would shift the invariant point to significantly lower pressure and steepen the slope of the corresponding univariant curves. Reactions which involve a melt phase have a subvertical slope whereas reactions that involve solid phases only have subhorizontal slopes. Therefore any *P–T* path that crosses melt-present reactions will have a shallower slope than a path in a grid whose reactions exclusively involve solid phases. As a result our retrograde path is dominated by cooling reactions compared to the one proposed by Tateishi et al. (2004), which is dominated by decompression reactions. Similar results were obtained by Moraes et al. (2002) for sapphirine–quartz rocks from Brazil who proposed a *P–T* path that also takes into account of melt-producing and melt-consuming reactions. They discuss in detail the role of melt in the evolution of the UHT granulites of central Brazil and located the melt-bearing invariant points [spinel,

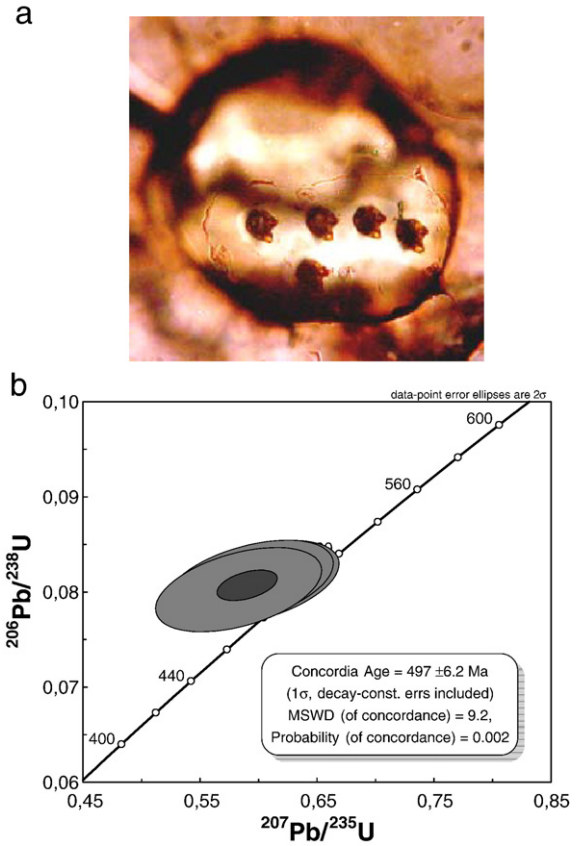

Fig. 7. a. Microphotograph of a monazite inclusion in garnet from sample I01-93-5 which has been dated by LA-ICP-MS at 501 ± 16 Ma. Width of individual spot sizes is 5 μm. b. Concordia diagram with individual U–Pb ages from the analysed monazite inclusion.

sapphirine] and [spinel, biotite] at similar pressures as in this paper (*ca*. 8–9 kbar).

The geochronological data presented in this study are consistent with the results of EPMA monazite dating recently presented by Braun and Appel (2006). They provide additional support for the occurrence of two stages of high-grade metamorphism in the Madurai Block during the early and late Neoproterozoic (*ca*. 900 and 550 Ma ago). The major challenge in interpreting these ages is to find a clear correlation between these age data and the metamorphic history that is recorded in the rocks which also host the monazites. In particular, a precise knowledge on the age of UHT metamorphism is crucial for a better understanding of the geodynamic evolution of the Madurai Block. Unfortunately, the results and observations which so far have been collected for the UHT granulites described in this study do not allow to unravel their *P*–*T*–*t* evolution unequivocally.

The slightly discordant Tonian age from the monazite inclusion in garnet could reflect a stage of UHT metamorphism that led to the development of the spr–qtz symplectite inclusions. The occurrence of monazite inclusions with such old relic cores in garnet and in proximity to the sapphirine–quartz symplectites could favour such an interpretation although the evidence for this correlation is not unequivocal. The heating–cooling path described in this paper could then reflect an early Neoproterozoic orogeny during which the studied granulite samples experienced a complex melting and mineral-melt back reaction sequence. In such a case and depending on the time of formation of the host garnet (very early according to reaction (1) or significantly later through reaction (5c)) the appropriate monazite ages represent maximum or minimum values for the time of UHT metamorphism, respectively. The rocks subsequently may have stayed in the lower continental crust and cooled down from ultra-high (>1000 °C) to high temperatures (~800 °C) before they were invaded by granitic melts during Pan-African orogeny and brought to a higher crustal level along a steep isothermal decompression path. Monazite and particularly spr–qtz intergrowths must have been shielded by garnet during this stage which allowed them to preserve their early Neoproterozoic geochronological and petrological features. Alternatively, one could argue that UHT metamorphism was related to Pan-African orogeny and occurred 550–600 Ma ago. We consider this explanation to be unlikely since in this case it would be difficult to explain that monazite was able to preserve ages older than 600 Ma although temperatures were well above

Table 4
U–Th–Pb ages from in-situ LA-ICP-MS dating of a monazite inclusion in garnet from the granulite sample I01-93-5

Spot #	Atomic ratios						Apparent ages							
	$^{206}Pb/^{238}U$	1σ	$^{207}Pb/^{235}U$	1σ	$^{208}Pb/^{232}U$	1σ	$^{206}Pb/^{238}U$	1σ	$^{207}Pb/^{235}U$	1σ	$^{208}Pb/^{232}U$	1σ	Concordia age	2σ
Ju29f04	0.082	0.002	0.599	0.030	0.026	0.001	510	11	477	24	514	14	–	–
Ju29f05	0.081	0.002	0.597	0.030	0.026	0.001	502	11	475	24	516	14	499	21
Ju29f06	0.080	0.002	0.583	0.029	0.024	0.001	498	11	467	23	487	13	495	21
Ju29f07	0.076	0.002	0.537	0.027	0.025	0.001	475	11	436	22	491	13	–	–
Ju29f08	0.081	0.002	0.592	0.029	0.025	0.001	502	11	472	23	499	13	499	21

common estimates for the closure temperature for Pb diffusion in monazite.

The late Neoproterozoic ages reported from monazite inclusions in quartz and orthopyroxene agree very well with available data from these rocks as well as from other places in the Southern Granulite Terrain (Santosh et al., 2003; Ghosh et al., 2004) and again confirm the widespread high-grade metamorphic event at the end of the Pan-African orogeny in this area.

Raith et al. (1997) provided a detailed petrologic study of sapphirine-bearing UHT granulites from the Palni Hills in southern India. Sapphirine–quartz assemblages were not observed but sillimanite pseudomorphs after kyanite point to significantly higher pressure (*ca*. 12 kbar) and slightly lower temperature (1000 °C) conditions than those reported in this study. Raith et al. (1997) proposed that the first stage of this path was dominated by high-*P* (*ca*. 12 kbar) isobaric heating and a high-*T* (*ca*. 1000 °C) isothermal decompression (down to *ca*. 8 kbar). Despite the lack of geochronological data they suggested that this stage took place during the Paleoproterozoic (*ca*. 2.5 Ga) and presumably was coeval with the tectono-metamorphic evolution of the Nilgiri, Biligiri Rangan and Shevaroy Hills.

Our geochronological data are in line with the possibility of two distinct orogenic events but do not show any evidence for a Paleoproterozoic stage of high-grade metamorphism as it is widespread in the granulite terrains further north in the SGT. This raises the question whether all sapphirine-bearing rocks in southern India have shared the same tectono-metamorphic evolution or not. Most of the rocks reflecting UHT conditions occur as enclaves or form small outcrops and yield a fairly wide range in *P–T* conditions and evolution. This as well as the fact, that with the exception of the data presented in this study, no texturally constrained geochronological information is available from these occurrences makes it difficult to judge if UHT metamorphism was a local or a regional phenomenon in the exposed crustal level of the SGT. Precise geochronology on the Palni Hills rocks could shed some light on the possible linkage between them and the Rajapalayam granulites. However, in both localities the last decompression stage (from 8 kbar), as recorded by the reaction of orthopyroxene and cordierite with melt-producing biotite, is agreed to take place at Pan-African times.

Magnesium- and aluminium-rich metapelites with similar sapphirine–quartz assemblages that indicate ultrahigh-temperature and medium to high pressure metamorphic conditions are reported from neighbouring Gondwana terrains in Sri Lanka and the Lützow–Holm Complex in Antarctica (Yoshimura et al., 2003; Osanai et al., 2006). They also occur as lenses or enclaves in ordinary pelitic gneisses and/or two-pyroxene granulites and charnockites. Merging observations in the host mafic granulites and the enclaves, Osanai et al. (2006) presented a *P–T* path that is dominated by two isothermal decompression stages. The occurrence of kyanite in the metapelites indicates significantly higher pressures (*ca*. 17 kbar) than in the rocks presented in this study and isothermal decompression to *ca*. 11 kbar, which was followed by isobaric cooling. Taking into account that the grids of Osanai et al. (2006) do not involve a melt phase, the pressure at which isobaric cooling occurs might be overestimated. The difference between the last segments of the isothermal decompression paths in Rajapalayam and Sri Lanka concerns spinel that is widely reported in symplectites and retrograde products in Sri Lankan rocks but clearly absent in the rocks studied in the South Indian UHT granulites. This might be explained by a model according to which the South Indian rocks cooled at depth (*ca*. 6 kbar), preventing the growth of retrograde spinel, whereas the Sri Lankan rocks were cooled during decompression (from *ca*. 6 kbar) to allow the widespread formation of spinel-bearing symplectites without entering the spinel–quartz stability field. On the other hand, it is known that oxygen fugacity plays a key role in the appearance of spinel, and the rocks from South India and Sri Lanka might have reequilibrated at different oxygen fugacity conditions. Osanai et al. (2006) report a high oxygen fugacity indicated by the coexistence of magnetite and spinel as well as the occurrence of magnetite exsolutions in spinel. The rocks found in Rajapalayam do no present such assemblages and probably have not seen spinel-bearing reactions as the bulk oxygen fugacity was too low.

UHT granulites from the Lützow–Holm Bay are interpreted to have evolved along a similar *P–T* path as the Sri Lankan occurrences (Yoshimura et al., 2003), which is characterised by isothermal decompression from a kyanite-stabilized granulite field through sapphirine+quartz, orthopyroxene+sillimanite and garnet–cordierite stability fields. Even though no precise geochronology has been undertaken on these rocks, Osanai et al. (2006) speculate that the localized UHT/HP metamorphism in the rocks from the Highland Complex and the Lützow–Holm Complex might have taken place before the Pan-African metamorphism. The correlation of the tectono-metamorphic evolution of these crustal fragments with that of UHT granulites in the Madurai Block in southern India has to be investigated by future studies.

Acknowledgements

We would like to thank the 'German Science Foundation' (DFG) and the 'German Academic Exchange Service' (DAAD) for research and travel grants (Br 1909/2–3 & -4; PROCOPE '312-ms'). B. Devouard is thanked for the minute micro-drilling of the minerals in this section. Careful and thorough reviews by Nigel Kelly and Renato Moraes helped to significantly improve the paper and are gratefully acknowledged.

References

Bartlett, J.M., Harris, N.B.W., Hawkesworth, C.J., Santosh, M., 1995. New isotope constraints on the crustal evolution of South India and Pan-African granulite metamorphism. Mem. Geol. Soc. India 34, 391–397.

Bartlett, J.M., Dougherty-Page, J.S., Harris, N.B.W., Hawkesworth, C.J., Santosh, M., 1998. The application of single zircon evaporation and Nd model ages to the interpretation of polymetamorphic terrains: an example from the Proterozoic mobile belt of south India. Contrib. Mineral. Petrol. 131, 181–195.

Bhaskar Rao, Y.J., Janardhan, A.S., Vijaya Kumar, T., Narayana, B.L., Dayal, A.M., Taylor, P.N., Chetty, T.R.K., 2003. Sm–Nd model ages and Rb–Sr isotope systematics of charnockites and gneisses across the Cauvery Shear Zone, Southern India: implications for the Archean–Neoproterozoic terrane boundary in the Southern Granulite Terrain. In: Ramakrishnan, M. (Ed.), Tectonics of Southern Granulite Terrain: Kuppam–Palani Geotransect. Memoir of the Geological Society of India, vol. 50, pp. 297–317.

Braun, I., Appel, P., 2004. Polymetamorphism in the Southern Granulite Terrain of India: implications from electron-microprobe dating of monazite. Eur. J. Mineral. 16, 23 (Beihefte).

Braun, I., Appel, P., 2006. U–Th-total Pb dating of orthogneisses and their ultra-high temperature metapelitic enclaves: implications for the multistage tectonic evolution in the Madurai Block, southern India. Eur. J. Mineral. 18, 415–428.

Brown, M., Raith, M., 1996. First evidence of ultrahigh-temperature decompression from the granulite province of southern India. J. Geol. Soc. (Lond.) 153, 819–822.

Carrington, D.P., Harley, S.L., 1995. Partial melting and phase relations in high-grade metapelites: an experimental petrogenetic grid in the KFMASH system. Contrib. Mineral Petrol. 120, 270–291.

Cenki, B., Kriegsman, L.M., 2005. Tectonics of the Neoproterozoic Southern Granulite Terrain, South India. Precambrian Res. 138, 37–56.

Cenki, B., Kriegsman, L.M., Braun, I., 2002. Melt-producing and melt-consuming reactions in the Achankovil cordierite gneisses, South India. J. Metamorph. Geol. 20, 543–561.

Chetty, T.R.K., Bhaskar Rao, Y.J., Narayana, B.L., 2003. A structural cross section along Krishnagiri–Palani Corridor, Southern Granulite Terrain of India. In: Ramakrishnan, M. (Ed.), Tectonics of Southern Granulite Terrain — Kuppam–Palani-Transect. Geological Society of India Memoir, vol. 50, pp. 255–278.

Dallwitz, W.B., 1968. Co-existing sapphirine and quartz in granulite from Enderby Land, Antarctica. Nature 219, 476–477.

Ellis, D.J., 1980. Osumilite–sapphirine–quartz granulites from Enderby Land, Antarctica; *P–T* conditions of metamorphism, implications form garnet–cordierite equilibria and the evolution of the deep crust. Contrib. Mineral. Petrol. 74, 201–210.

Ghosh, J.P., de Wit, M.J., Zartman, R.E., 2004. Age and tectonic evolution of Neoproterozoic ductile shear zones in the Southern Granulite Terrain of India, with implications for Gondwana studies. Tectonics 23, TC3006. doi:10.1029/2002TC001444.

Grew, E.S., 1982. Sapphirine, kornerupine, and sillimanite + orthopyroxene in the charnockitic region of South India. J. Geol. Soc. India 23, 469–505.

Harley, S.L., 1998. On the occurrence and characterization of ultrahigh-temperature crustal metamorphism. In: Treloar, P.J., O'Brien, P.J. (Eds.), What Drives Metamorphism and Metamorphic Reactions? . Geological Society, London, Special Publications, vol. 138, pp. 81–107.

Harley, S.L., Green, 1982. Garnet–orthopyroxene barometry for granulites and peridotites. Nature 300, 697–701.

Harris, N.B.W., Santosh, M., Taylor, P.N., 1994. Crustal evolution in South India: constraints from Nd isotopes. J. Geol. 102, 139–150.

Jayananda, M., Janardhan, A.S., Sivasubramanian, P., Peucat, J.-J., 1995. Geochronologic and isotopic constraints on granulite formation in the Kodaikanal area, southern India. In: Yoshida, M., Santosh, M. (Eds.), India and Antarctica during the Precambrian. Geol. Soc. India Memoir, vol. 34, pp. 373–390.

Kelsey, D.E., White, R.W., Holland, T.J.B., Powell, R., 2004. Calculated phase equilibria in K_2O–FeO–MgO–Al_2O_3–SiO_2–H_2O for sapphirine–quartz-bearing mineral assemblages. J. Metamorph. Geol. 22, 559–578.

Kretz, R., 1983. Symbols for rock-forming minerals. Am. Mineral. 68, 277–279.

Kriegsman, L.M., Hensen, B.J., 1998. Back reaction between restite and melt: implications for geothermobarometry and pressure–temperature paths. Geology 26, 1111–1114.

McDade, P., Harley, S.L., 2001. A petrogenetic grid for aluminous granulite facies metapelites in the KFMASH system. J. Metamorph. Geol. 19, 45–59.

Miller, J.S., Santosh, M., Pressley, R.A., Clements, A.S., Rogers, J.J.W., 1997. A Pan-African thermal event in southern India. J. Southeast Asian Earth Sci. 14, 127–136.

Mohan, A., Windley, B.F., 1993. Crustal trajectory of sapphirine-bearing granulites from Ganguvarpatti, South India: evidence for an isothermal decompression path. J. Metamorph. Geol. 11, 867–878.

Moraes, R., Brown, M., Fuck, R.A., Camargo, M.A., Lima, T.M., 2002. Characterization and *P–T* evolution of melt-bearing ultrahigh-temperature granulites: an example from the Anapolis–Itauçu Complex of the Brasilia Fold belt, Brazil. J. Petrol. 43, 1673–1705.

Osanai, Y., Sajeev, K., Owada, M., Kehelpannala, K.V.W., Prame, W.K.B., Nakano, N., Jayatileke, S., 2006. Metamorphic evolution of high-pressure and ultra-high-temperature granulites from the Highland Complex, Sri Lanka. J. Asian Earth Sci. 28, 20–37.

Paquette, J.L., Pin, C., 2001. A new miniaturized extraction chromatography method for precise U–Pb zircon geochronology. Chem. Geol. 176/1–4, 313–321.

Paquette, J.L., Tiepolo, M., in press. High resolution (5 μm) U–Th–Pb isotope dating of monazite with excimer laser ablation (ELA)-ICP-MS. Chemical Geology.

Paquette, J.-L., Goncalves, P., Devouard, B., Nicollet, C., 2004. Micro-drilling ID-TIMS U–Pb dating of single monazites: a new method to unravel complex poly-metamorphic evolutions. Application to the UHT granulites of Andriamena (North-Central Madagascar). Contrib. Mineral. Petrol. 147, 110–122.

Pouchou, J.L., Pichoir, F., 1984. A new model for quantitative X-ray microanalysis, Part I: application to the analysis of homogeneous samples. La Recherche Aérospatiale, vol. 3, pp. 167–192.

Raith, M., Karmakar, S., Brown, M., 1997. Ultra-high-temperature metamorphism and multistage decompressional evolution of sapphirine granulites from the Palni Hill Ranges, southern India. J. Metamorph. Geol. 15, 379–399.

Sajeev, K., Osanai, Y., Santosh, M., 2004. Ultrahigh-temperature metamorphism followed by two-stage decompression of garnet–orthopyroxene–sillimanite granulites from Ganguvarpatti, Madurai block, southern India. Contrib. Mineral. Petrol. 148, 29–46.

Santosh, M., Yokoyama, K., Biju-Sekhar, S., Rogers, J.J.W., 2003. Multiple tectonothermal events in the granulite blocks of southern India revealed from EPMA dating: implications on the history of supercontinents. Gondwana Res. 6, 29–63.

Santosh, M., Tsunogae, T., Koshimoto, S., 2004. First report of sapphirine-bearing rocks from the Palghat–Cauvery Shear Zone system, southern India. Gondwana Res. 7, 620–626.

Satish-Kumar, M., 2000. Ultrahigh-temperature metamorphism in Madurai granulites, southern India: evidence from carbon isotope thermometry. J. Geol. 108, 479–486.

Spear, F.S., Kohn, M.J., Cheney, J.T., 1999. *P–T* paths from anatectic pelites. Contrib. Mineral. Petrol. 134, 17–32.

Stacey, J.S., Kramers, J.D., 1975. Approximation of terrestrial lead isotope evolution by a two-stage model. Earth Planet. Sci. Lett. 26, 207–221.

Tateishi, K., Tsunogae, T., Santosh, M., Janardhan, A.S., 2004. First report of sapphirine+quartz assemblage from southern India: implications for ultrahigh-temperature metamorphism. Gondwana Res. 7, 899–912.

Tiepolo, M., 2003. In situ Pb geochronology of zircon with laser ablation-inductively coupled plasma-sector field mass spectrometry. Chem. Geol. 192, 1–19.

van Achterbergh, E., Ryan, C.G., Jackson, S.E., Griffin, W., 2001. Data reduction software for LA-ICP-MS. In: Sylvester, P. (Ed.), Laser Ablation-ICPMS in the Earth Sciences. Mineralogical Association of Canada Short Course, vol. 29, pp. 239–243.

Yoshimura, Y., Motoyoshi, Y., Miyamoto, T., 2003. Sapphirine-bearing garnet–orthopyroxene granulite from Rundvagshetta in the Lützow–Holm Complex, East Antarctica. Abstract of the 23rd Symposium on Antarctica Geosciences. National Institute of Polar Research, Japan, p. 74.

Zen, E.-An, 1966. Construction of pressure–temperature diagrams for multicomponent systems after the method of Schreinemakers: a geometric approach. U.S. Geol. Surv. Bull. 1225, 1–56.